molecular pharmaceutics

pubs.acs.org/molecularpharmaceutics

Article

Fast-Disintegrating Nanofibrous Web of Pullulan/Griseofulvin−Cyclodextrin Inclusion Complexes

Emmy Hsiung, Asli Celebioglu,* Mehmet Emin Kilic, Engin Durgun, and Tamer Uyar*

Cite This: https://doi.org/10.1021/acs.molpharmaceut.3c00074

Read Online

ACCESS | Metrics & More | Article Recommendations | Supporting Information

ABSTRACT: Griseofulvin (GSF) is one of the most widely used antifungal suffering from low water solubility and limited bioavailability. Here, cyclodextrin (CD) derivatives of hydroxypropyl-beta-CD (HPβCD) known for its high-water solubility were used to form inclusion complexes (ICs) with GSF. Here, the molecular modeling study revealed the more efficient complex formation with 1:2 (guest:CD) stoichiometry, so ICs of GSF-HPβCD were prepared using a 1:2 molar ratio (GSF:HPβCD) and then mixed with pullulan (PULL) to generate nanofibers (NFs) using the electrospinning technique. PULL is a nontoxic water-soluble biopolymer and the ultimate PULL/GSF-HPβCD-IC NF was obtained with a defect-free fiber morphology having 805 ± 180 nm average diameter. The self-standing and flexible PULL/GSF-HPβCD-IC NF was achieved to be produced with a loading efficiency of ∼98% corresponding to ∼6.4% (w/w) of drug content. In comparison, the control sample of PULL/GSF NF was formed with a lower loading efficiency value of ∼72% which equals to ∼4.7% (w/w) of GSF content. Additionally, PULL/GSF-HPβCD-IC NF provided an enhanced aqueous solubility for GSF compared to PULL/GSF NF so a faster release profile with ∼2.5 times higher released amount was obtained due to inclusion complexation between GSF and HPβCD within the nanofibrous web. On the other hand, both nanofibrous webs rapidly disintegrated (∼2 s) in the artificial saliva medium that mimics the oral cavity environment. Briefly, PULL/GSF-HPβCD-IC NF can be a promising dosage formulation as a fast-disintegrating delivery system for antifungal oral administration owing to the improved physicochemical properties of GSF.

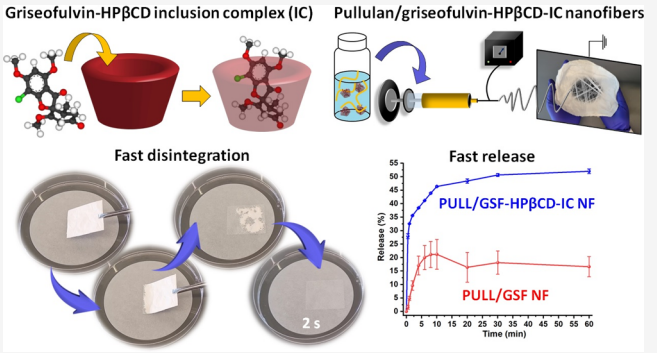

KEYWORDS: *cyclodextrin, electrospinning, pullulan, griseofulvin, antifungal, fast disintegrating drug delivery*

1. INTRODUCTION

Oral drug delivery methods, such as tablets and capsules, are a widely used means of drug administration due to their ease of administration and general acceptance by patients.[1] Tablet dosage forms are not always a viable way for patients (pediatric or geriatric) who can have trouble during swallowing pills. Therefore, fast disintegrating delivery systems (FDDSs) in the formula of films, patches, or tablets have gained attention in the pharmaceutical industry.[2,3] The active pharmaceutical ingredients (APIs) incorporated in FDDSs can be quickly disintegrated by the mucosa in the oral cavity and ensure a fast release of APIs without risk of chocking.[4] By this way, the first-pass metabolism of drugs which are known with limited aqueous solubility and bioavailability can be eliminated and so a higher absorption of these drugs can be ensured in the body.[1−4] The nanofibrous webs generated by using the electrospinning technique enable the encapsulation of APIs and so have drawn great attention to develop FDDSs owing to attractive advantages of nanofibers (NFs) including very porous structure, much higher ratio of surface area-to-volume, light-weight, etc. Here, different types of release profiles can be obtained by manipulating the electrospinning components and techniques.[5,6] For instance, studies report the incorporation of APIs into electrospun nanofibrous webs for potential FDDS administration of anti-inflammatory drugs,[7] supplements,[8] analgesics,[9] chemotherapy medications,[10] etc. The amorphization of APIs and their uniformly noncrystalline distribution within the NF carrier matrix are the principally attractive advantages for developing FDDSs.

For FDDS, both natural and synthetic polymers can be used which should have water-soluble, nontoxic, and nonirritating properties.[3] Therefore, polysaccharides are broadly applied for developing biomaterials, since they are biocompatible, biodegradable, and nontoxic.[11] The amorphization of APIs in the case of electrospinning can be achieved by very fast

Received: January 27, 2023
Revised: March 22, 2023
Accepted: March 23, 2023

evaporation of the solvent during the electrospinning process.[12] In this study, pullulan (PULL) was chosen as the polymeric template, which is a well-known linear polysaccharide having repeating maltotriose units.[13] PULL is obtained from the fungus *Aureobasidium pullulans*. Differently from other polysaccharide types, PULL can easily dissolve in water thanks to the low degree of hydrogen bonding in the structure.[14] It has been previously reported that electrospun nanofibrous webs of PULL can be used for drug transportation,[15] filtration,[16] medical scaffolds,[17] and food packaging.[18−21] PULL can also be electrospun into NFs along with the combination of a variety of drug molecules to create FDDSs.[22,23]

It is well-known that cyclodextrins (CDs), oligosaccharides in cyclic shape, significantly increase the water-solubility and improve the physicochemical properties of drug molecules by forming noncovalent inclusion complexes (ICs).[24,25] Thereby, CDs have become a favorable way to enhance the potential of poorly water-soluble drug molecules.[26] The chemically modified CD of hydroxypropyl-beta-CD (HPβCD) is especially favorable for drug formulations due to its significant water solubility.[27,28] HPβCD has been researched for animal/human trials, and it has been detected that this CD type can be well tolerated particularly for oral treatment.[29,30] The solubility of different drug molecules, such as antibiotics,[31] antivirals,[32] antiemetics,[33] steroids,[34] etc., can be enhanced by complexation with HPβCD and this makes it a suitable candidate to form FDDSs.

Griseofulvin (GSF), being an antifungal drug, is produced from the fungus *Penicillium griseofulvum* and is used orally to treat tinea disease for infections.[35] GSF has a low solubility in water of 8.64 mg/L, leading to low bioavailability and limited absorption in the body and another drawback is its bitter taste, which may be problematic for liquid administration, as is common for pediatric patients.[35−37] The commercial dosage forms of GSF are micro or ultramicro size tablets and liquid suspensions.[38] The therapy duration for these dosage forms can reach 12 weeks and this is a long period that can cause noncompliance for the patient during the treatment.[38] Therefore, there is still demand for new dosage forms of GSF which can provide a faster therapeutic action while ensuring patient compliance. At this point, FDDSs in the form of electrospun nanofibrous substrates can be a potential solution worthy of exploration. Moreover, studies have shown that water solubility enhancement and increase in the bioavailability of GSF were successful by forming ICs with GSF and CD molecules.[28,36,39] Additionally, different nanoformulation approaches including nanosponges, nanoparticles, NFs, etc. have been adapted with and without the use of CD, to address the low bioavailability and low solubility issues of GSF.[35−37] For instance, the encapsulation of GSF into electrospun polyvinylpyrrolidone (PVP) NF for the purpose of potential FDDS was studied.[35−37] However, the toxic solvent systems, ethanol/dimethylacetamide (DMAc) and acetone/DMAc, were used to dissolve GSF and carrier polymer (PVP) in electrospinning solutions. On the other hand, the aim of this study is to produce NF-based PULL/GSF-HPβCD-ICs as FDDSs which can be an alternative to the conventional drug dosage form of antifungals by using nontoxic and "green" components (Figure 1). In addition, PULL/GSF NFs were produced to serve as the control sample. The structural examination, disintegration behavior, and *in vitro* release tests of samples were performed by additional techniques.

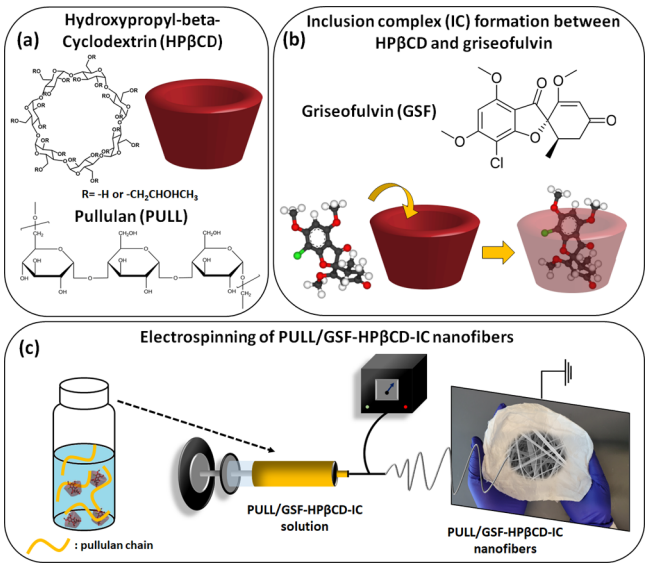

Figure 1. Presentation of (a) HβCD and PULL chemical structure, (b) inclusion complexation between HβCD and GSF molecule, and (c) the electrospinning process for PULL/GSF-HPβCD-IC NFs.

2. MATERIALS AND METHODS

2.1. Materials. Wacker Chemie AG (USA) gifted HPβCD (*CAVASOL W7* HP, DS: ∼0.9−95.0%) for scientific research. GSF (TCI America − >97.0% HPLC), PULL having molecular weight of 300,000 g/mol (TCI America − 92.0%), dimethyl sulfoxide (DMSO) (Sigma, >99.9%), deuterated DMSO (DMSO-d6) (Cambridge Isotope, 99.8%), and phosphate buffered saline tablet (Sigma) were used as is without any purification steps. Water used was from a Millipore Milli-Q ultrapure system (Millipore − USA).

2.2. Computational Methodology. The density functional theory (DFT) analyses within this study were computed by using ab initio approaches.[8,40] The projector augmented potentials with 520 eV energy cutoff were used to represent element potentials. The generalized gradient approximation (GGA-PBE) was employed to approximate the exchange-correlation term. The long-range dispersion interactions were calculated by the DFT-D2 approach.[41] The HPβCD and GSF structures were relaxed into their ground state configurations by a conjugate-gradient algorithm setting 10^{-5} eV as the energy and 5 meV/Å as force convergence limit. The calculations were repeated in water by adapting the implicit solvation technique.[42]

2.3. Phase Solubility. In order to investigate the solubility behavior of GSF with HPβCD, a predetermined amount of GSF was mixed with HPβCD using increasing concentrations of CD (0−128 mM) in water (5 mL). The solutions were shaken by an orbital shaker at 450 rpm speed for 24 h at room temperature (RT) by using shielding from any light source. Then, these solutions were filtered by using a filter (0.45 μm, polytetrafluoroethylene (PTFE)). UV−vis spectroscopy (Perkin Elmer − Lambda 35 − USA) was used for the absorbance measurement of each aliquot at 294 nm. This experiment was repeated three times.

2.4. Electrospinning. First, 1:2 (GSF:HPβCD) molar ratio was used to form ICs between GSF and HPβCD. Here,

https://doi.org/10.1021/acs.molpharmaceut.3c00074
Mol. Pharmaceutics XXXX, XXX, XXX−XXX

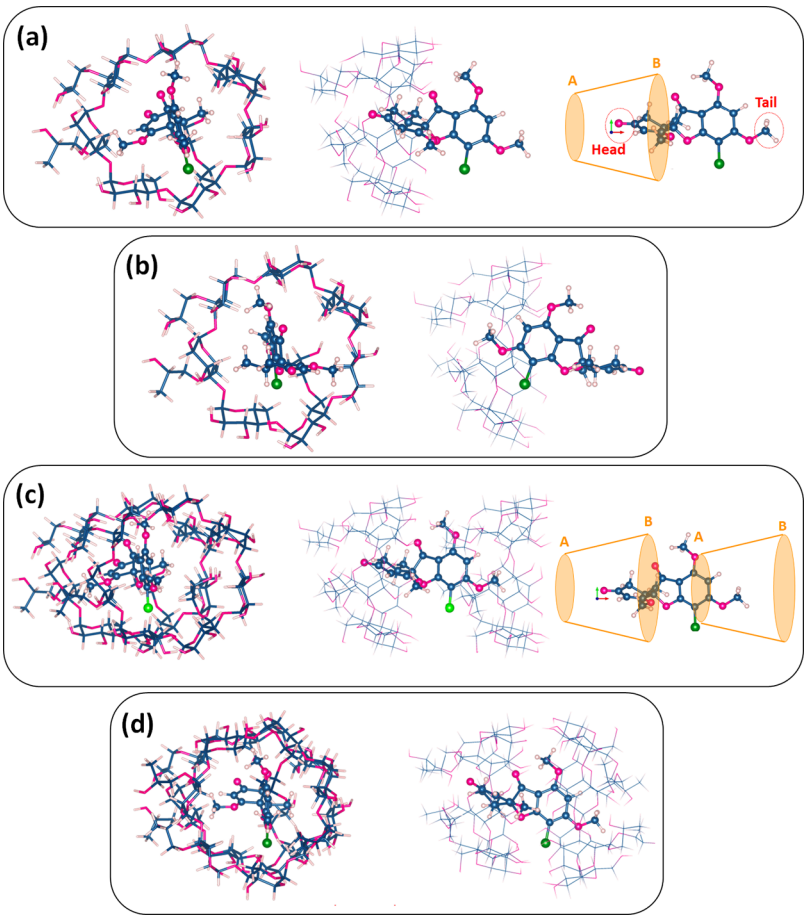

Figure 2. Top/side views of (a, b) 1:1 and (c, d) 1:2 configurations of GSF:HPβCD-IC.

HPβCD (20%, w/v) (~400 mg) was dissolved in water (2 mL), then GSF powder (~47 mg) was added to this solution and allowed to stir overnight (RT). Afterward, PULL (15% (w/v) (~300 mg) was included into the GSF-HPβCD-IC solution (at RT). Here, pristine PULL (20% (w/v)), PULL/HPβCD (15%/20% (w/v)), and PULL/GSF (15% (w/v)) were prepared as control samples. PULL/GSF was loaded with the same drug ratio of GSF (6.5%, w/w) similar to PULL/GSF-HPβCD-IC. The conductivity and viscosity of electrospinning systems were determined before the process. The FiveEasy conductivity-meter (Mettler Toledo-USA) was used for the measurements of the conductivity value of electrospinning solutions (RT). The rheometer (AR 2000 rheometer, TA Instrument, USA) measurements were performed under these conditions: cone-plate spindle: 20 mm with 4°; shear rate: 0.01 to 1000 s^{-1}; temperature: 20 °C, to determine the viscosity of the solutions. For electrospinning, each solution was loaded into a syringe (1 mL, having 27 G needle). Then, the electrospinning (Spingenix-SG100, Palo Alto-USA) was performed under the environmental conditions of 21 °C and 23% relative humidity. The high voltage within the range of 13 to 17 kV was applied, whereas the flow rate of the solutions was varied between 0.7 and 1.0 mL/h, depending on the solutions used. The samples of NFs were collected on a metal platform covered with an aluminum foil where the collection distance was set to 15 cm.

2.5. Structural Analysis. The morphological analyses of the samples, PULL/GSF-HPβCD-IC NF and PULL/GSF NF, PULL/HPβCD NF, and PULL NF, were carried out by scanning electron microscopy (SEM) (Tescan-MIRA3, Czech Republic). The average fiber diameter (AFD) was obtained by calculating ~100 NFs from SEM images and using ImageJ software. The Fourier transform infrared (FTIR) spectra for GSF crystalline powder, HPβCD white powder, and NF samples were recorded by FTIR-attenuated total reflectance (PerkinElmer-USA) in the range of 4000−600 cm^{-1} with a resolution of 4 cm^{-1} by averaging a total of 32 scans. X-ray diffractometry (BrukerD8 Advance ECO, USA) was used to determine the X-ray diffraction patterns of the same samples (2θ: 10°−30° − Cu/Kα radiation − 40 kV and 25 mA). The overall thermal properties of GSF, HPβCD, and NF samples were analyzed and compared by using thermal characterization methods: differential scanning calorimetry (DSC) (Q2000, TA Instruments, USA) (Tzero aluminum pan, rate: 10 °C/min, range: 0 °C−250 °C - N_2) and thermogravimetric analysis (TGA) (Q500, TA Instruments, USA) (platinum pan, rate: 20 °C/min, range: 30−600 °C − N_2).

The loading efficiency of PULL/GSF-HPβCD-IC NF and PULL/GSF NF was determined by dissolving a fixed amount of sample (~1 mg) in DMSO (3 mL). Here, DMSO was chosen to ensure the complete dissolution of all components of the NFs including PULL, HPβCD, and GSF. UV−vis spectroscopy (292 nm) was used to check the GSF content in the nanofibrous webs. The calibration curve of GSF in DMSO was obtained with $R^2 \geq 0.99$. The loading efficiency (%) was determined as:

$$\text{Loading efficiency}\ (\%) = C_e/C_t \times 100 \quad (1)$$

https://doi.org/10.1021/acs.molpharmaceut.3c00074
Mol. Pharmaceutics XXXX, XXX, XXX−XXX

Table 1. GSF:HPβCD-IC Complexation/Solvation Energies for Tail (T) and Head (H) Orientations of GSF Considering Both 1:1 and 1:2 Stoichiometries[a]

stoichiometry	orientation	E_{CE}^{Vacuum} kcal/mol	E_{CE}^{Water} kcal/mol	E_{SE} kcal/mol
1:1	AB-HT	12.44	6.45	−68.70
	AB-TH	7.76		
1:2	AB-HT-AB	30.14		
	AB-HT-BA	75.43	32.91	−98.04

[a]A (narrow rim) and B (wide rim) express the orientation of HPβCD as shown in Figure 2.

where C_e and C_t are defined as the concentration of loaded GSF and initial concentration of GSF, respectively. The experiments were repeated three times.

2.6. Dissolution Test. UV−vis spectroscopy was performed for the dissolution test of PULL/GSF-HPβCD-IC NF and PULL/GSF NF. Each NF having a similar amount of GSF (∼10 mg for PULL/GSF-HPβCD-IC NF and ∼13.5 mg for PULL/GSF NF) was dissolved in PBS buffer (5 mL) on an orbital shaker (200 rpm − RT) for 10 min. Then, these solutions were filtered using a PTFE filter (0.45 μm). The UV−vis spectra were recorded (294 nm), and the experiment was repeated three times.

2.7. Time-Dependent Release Test. For examining the time-dependent drug release from the samples, the same amount of PULL/GSF-HPβCD-IC NF and PULL/GSF NF (∼10 mg) was dipped into PBS buffer (pH 7.4) solution (10 mL) and then was shaken by using the orbital shaker at a speed of 200 rpm at RT. For the predetermined time intervals, 1 mL of aliquot was taken from each system followed by the addition of 1 mL of fresh PBS buffer. Afterward, UV−vis measurements were performed to determine the time-dependent release of the GSF amount (%). The measurements were repeated three times. The release kinetic was further studied by using various models (Supporting Information).

2.8. Disintegration Test. To test the disintegration of PULL/GSF-HPβCD-IC NF and PULL/GSF NF, artificial saliva (pH 6.8)[33] simulating the oral cavity was used. Here, the disintegration test was conducted by placing the filter paper in a Petri dish (10 cm) and then wetted with artificial saliva solution (10 mL). The excessed solution was drained out of the Petri dish and then samples (∼2.5 cm × 3.0 cm − ∼10 mg) were gently placed on the filter paper and the video was recorded simultaneously (Video S1).

2.9. Statistical Analysis. For repeated experiments, the one-way or two-way analysis of variance (ANOVA) was performed for statistical analysis (OriginLab (Origin 2022b, USA)). Tukey's comparison test was applied to detect the difference between results ($p \leq 0.05$).

3. RESULTS AND DISCUSSION

3.1. Molecular Modeling Analysis. The formation of the IC between HPβCD and GSF was examined with first-principles calculations. As a first step, HPβCD and GSF were designed and then optimized separately to obtain the ground state configurations. Next, their interaction was analyzed as a function of distance beginning with 1:1 (GSF:HPβCD) stoichiometry. It was noticed that the total energy of the system decreased as GSF approached HPβCD, indicating that the binding was energetically favorable. For the IC formation, the orientation of the GSF and HPβCD affected the strength of interaction. As the narrow rim (A) of HPβCD was partially covered by HP arms, GSF entered HPβCD through the wide rim (B). Although GSF could not vertically fit into HPβCD due to length molecule (∼12.1 Å), horizontal orientation (head (H) or tail (T)) was possible for complex formation (Figure 2a,b). The complexation energy (E_{comp}), which is a measure of interaction strength, can be computed when the total energy of the system reaches its minimum. The below formula:

$$E_{comp} = n \times E_T[\text{host}] + E_T[\text{guest}] - E_T[\text{IC}] \quad (2)$$

in which the terms defined as E_T[host], E_T[molecule], and E_T[IC] are the ground state energies of HPβCD, GSF, and GSF-HPβCD-IC, respectively. n refers to the number of HPβCD and is equal to 1 (2) for 1:1 (1:2) stoichiometry. As can be seen from Table 1, E_{comp} for head orientation is larger than that calculated for the tail orientation. Our results indicated that in addition to 1:1, ICs can also be formed in 1:2 stoichiometry (Figure 1c,d). In this case, the lowest energy configuration was attained when head and tail ends of GSF interacted with the wide rims of both HPβCD. When compared, E_{comp} (1:2) was significantly larger than E_{comp} (1:1) indicating that 1:2 is a more favorable configuration for the IC (Table 1). To reveal the solvent effect, the calculations were repeated in water. Although the structures remained the same, a considerable decrease in E_{comp} was noticed, which implied a weakening in binding strength among GSF and HPβCD. Comparing the difference in total energies that are obtained in vacuum and water, the solvation energy (E_{solv}) of the IC can be estimated. These analyses showed that the E_{solv} of GSF increased from −8.8 kcal/mol up to −68.7 kcal/mol for 1:1 and −98.0 kcal/mol for 1:2 configurations, respectively (Table 1). The increase in E_{solv} together with the decrease in E_{comp} in water pointed out an enhancement in solubility.

3.2. Phase Solubility Analysis. The data from phase solubility analysis for GSF were plotted in the range of 0−128 mM CD concentration which is an A_L-type diagram that shows the linear increase of solubility of GSF against increasing CD concentration in the given range (Figure S1).[43] The aqueous solubility of GSF is ∼0.035 mM, which increased to ∼0.13 mM at the highest concentration of HPβCD, for an overall increase by a factor ∼3.7. From this experimental analysis, the binding constant value (K_s) for the IC of GSF/HPβCD was calculated as 20 M^{-1}. These results aligned with those of Veiga et al. which classified the phase solubility profile of GSF and HPβCD as a type A_L, and the binding constant in their experiment was found to be 12 M^{-1}.[39] While the binding constant found by Veiga et al. is slightly lower than found here, it is fairly close, and the diagram types are consistent. Overall, the solubility of GSF was found to increase with increasing concentration of HPβCD.

3.3. Morphology Analysis. Based on the findings from the molecular modeling analysis, the molar ratio of 1:2 (GSF:HPβCD) was used for forming the IC between HPβCD and GSF, and this corresponds to ∼6.5% (w/w) of GSF in the

https://doi.org/10.1021/acs.molpharmaceut.3c00074
Mol. Pharmaceutics XXXX, XXX, XXX−XXX

Table 2. Composition and Properties of Electrospinning Solutions and Fiber Diameter of the Electrospun Samples

sample	PULL conc. (%, w/v)[a]	HPβCD conc. (%, w/v)[a]	GSF conc. (%, w/w)[b]	viscosity (Pa·s)	conductivity (μS/cm)	average fiber diameter (nm)
PULL	20			0.489	38.3	590 ± 95
PULL/HPβCD	15	20		0.296	123.8	705 ± 155
PULL/GSF-HPβCD-IC	15	20	6.5	0.322	126.3	805 ± 180
PULL/GSF	15	20	6.5	0.237	39.0	290 ± 60

[a]According to the solvent (water). [b]According to the total sample amount.

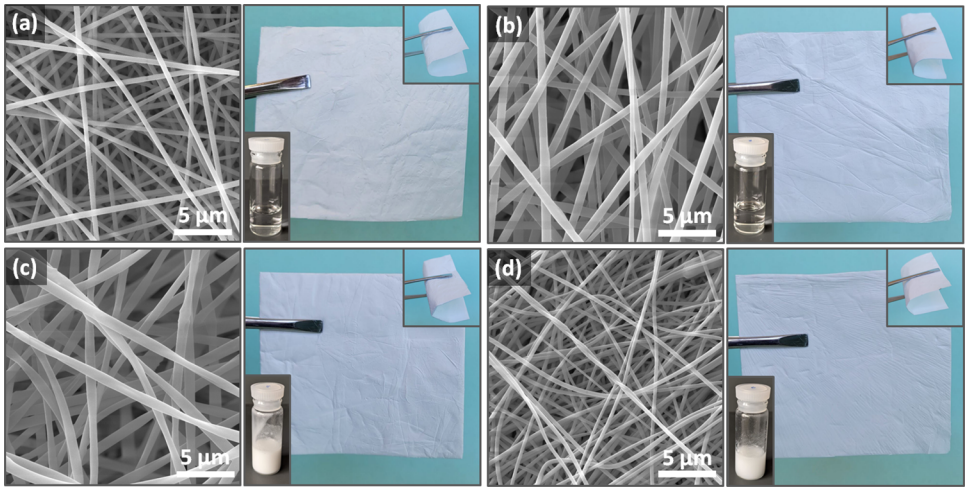

Figure 3. Representative SEM views (left) and photos (right) of process solutions and nanofibrous webs of (a) PULL NF, (b) PULL/HPβCD NF, (c) PULL/GSF-HPβCD-IC NF, and (d) PULL/GSF NF.

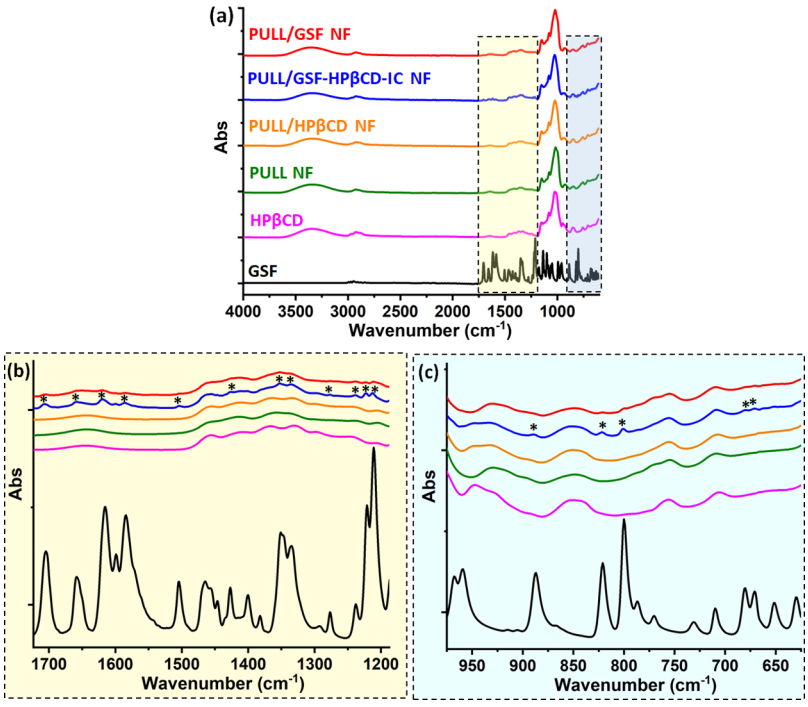

Figure 4. FTIR spectra of (a) full region, and (b, c) the expanded region of GSF, HPβCD, PULL NF, PULL/HPβCD NF, PULL/GSF-HPβCD-IC NF, and PULL/GSF NF.

electrospun NF samples. The concentration of each component used within samples is mentioned in Table 2. The solution properties and the AFD values are also given in Table 2. In addition, SEM images given in Figure 3 indicated that all electrospinning systems returned into defect-free nanofibrous webs, which were also self-standing and flexible. The pristine PULL and PULL/HPβCD solutions (Figure 3a,b) are clear; in contrast, PULL/GSF-HPβCD-IC and PULL/GSF solutions (Figure 3c,d) are white due to the uncomplexed drug content in the solutions. It can be seen that the addition of HPβCD resulted in a noteworthy increase in the conductivity, while the addition of GSF barely increased

https://doi.org/10.1021/acs.molpharmaceut.3c00074
Mol. Pharmaceutics XXXX, XXX, XXX−XXX

the conductivity of the systems. Here, PULL/GSF-HPβCD-IC NFs had a thicker fiber than PULL/HPβCD NFs. The PULL/GSF-HPβCD-IC solution had a higher viscosity and the two solutions had similar conductivities, so the viscosity would largely influence the fiber diameter, with the more viscous solution resulting in a thicker fiber due to less stretching thru electrospinning.[44] When comparing the pristine PULL solution to the PULL/GSF one, it can be seen that conductivities were similar, but the viscosity of the PULL/GSF solution was lower. This was due to lower concentration of PULL (15%, w/v) that was used for the electrospinning of the PULL/GSF system when compared to the pristine PULL system (20%, w/v). This data also correlated with the previous reports where lower viscosity solutions produce much thinner fibers as a result of higher stretching of the jet, and contrarywise higher viscosity solutions produce thicker fibers during the electrospinning process.[44] The statistical analyses revealed the significant differences between the average fiber diameter values of electrospun nanofibrous webs ($p < 0.05$)). It is noteworthy to mention that both PULL/GSF-HPβCD-IC and PULL/GSF nanofibrous webs kept their structural features such as still being self-standing and flexible even after 20 months of storage in a refrigerator (+4 °C) without the need for a special packaging. This finding reveals the long-term stability of PULL/GSF-HPβCD-IC NF during storage (Figure S2).

3.4. Structural Characterization. Figure 4 shows the FTIR graphs of samples both in full and expanded scales. For HPβCD, the absorption bands of C−C/C−O stretching, C−O−C glycosidic bridge stretching, $-CH_3$ bending, O−H bending, C−H stretching, and −OH stretching in the structure led to the observation of peaks at 1028, 1150, 1180, 1650−1370, 2930, and 3324−3355 cm^{-1}, respectively (Figure 4a).[45] The FTIR profile of PULL and HPβCD was analogous in the spectrum because of their similar chemical structures (glucose and glucopyranose units). PULL NF indicated absorption peaks at 3313, 2925, 1641, and 1200−1000 cm^{-1} which correspond to the ν(O−H) stretching, ν(C−H) stretching, H−O−H bending, and intense ν(C−O) stretching, respectively (Figure 4a).[23,46] In the case of GSF, there were characteristic absorption bands at 1703 cm^{-1} corresponding to C═O stretching; 1657 and 1426 cm^{-1} due to C═C bending of the benzene ring; 1212 cm^{-1} corresponding to C−O bending; and 820 cm^{-1} from C−Cl bending (Figure 4b,c).[36] These distinct peaks were found in PULL/GSF-HPβCD-IC NF and PULL/GSF NF, indicating the successful incorporation of the drug into the NFs. The absorption was more intense in the PULL/GSF-HPβCD-IC NF than the PULL/GSF NF, which may be due to a possible higher content of GSF in the NF originated by the inclusion complexation that will be discussed in the following section.

The X-ray diffraction measurement was carried out to observe the crystallinity of samples. Figure 5a shows the X-ray diffraction (XRD) graphs of GSF, HPβCD, and electrospun samples. GSF had numerous distinct peaks found at 10.8°, 13.3°, 14.6°, 16.6°, 23.9°, and 26.7° as was expected of crystalline materials. In contrast, the broad halo diffraction pattern demonstrating that both HPβCD and PULL have an amorphous structure (Figure 5a). As it was shown in the previous part, the GSF loaded PULL solutions prepared with/without HPβCD had both turbid view because of the existence of uncomplexed and crystal GSF in the system. Consequently, the ultimate electrospun samples from these solutions were expected to include GSF crystals. As anticipated, the diffraction

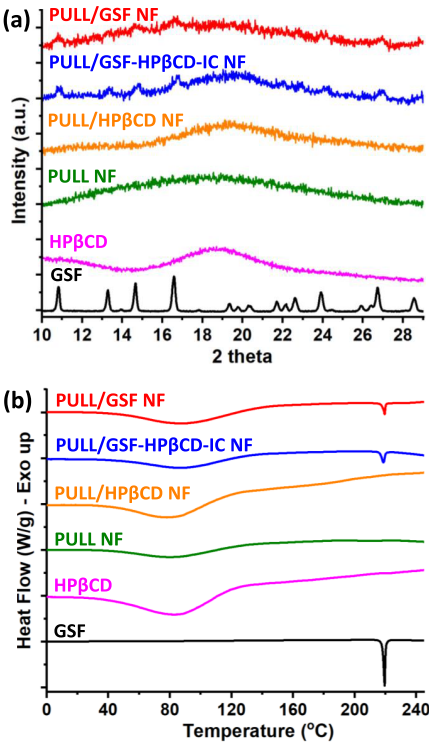

Figure 5. Data of (a) XRD and (b) DSC of GSF, HPβCD, PULL NF, PULL/HPβCD NF, PULL/GSF-HPβCD-IC NF, and PULL/GSF NF.

peaks of GSF were found in the XRD graphs of PULL/GSF-HPβCD-IC NF and PULL/GSF NF signifying the presence of the drug crystals in these samples. As reported in the earlier studies, the IC formation with CD molecules can transform the crystal state of the drug into amorphous one.[23,31,33,34] Here, the encapsulation of drug molecules into the CD void prevents the re-packing of these molecules into the crystal assembly again. However, it was found that PULL/GSF-HPβCD-IC NF displayed the characteristic peaks of GSF due to uncomplexed drug parts in this nanofibrous web.[37] To reveal a relative comparison between samples, the integral areas of the XRD graphs of PULL/GSF-HPβCD-IC NF and PULL/GSF NF were examined using OriginLab. Here, the relative crystal ratio of PULL/GSF-HPβCD-IC NF (~6.3%) was found to be lower compared to PULL/GSF NF (~10.3%) and this might be evidence for the higher crystal drug content of PULL/GSF NF than PULL/GSF-HPβCD-IC NF.

DSC findings can also shed light on the crystalline structure of the drug and NFs. In the DSC of GSF (Figure 5b), a sharp endothermic peak was observed at 219.4 °C that corresponds to the melting point of GSF and its highly crystalline nature. On the other hand, the DSC thermograms of HPβCD and PULL did not indicate a distinct endothermic peak of melting point due to the amorphous nature of HPβCD and PULL. For all samples, except GSF powder, the endothermic peaks observed at around 80 to 85 °C correspond to the dehydration process. Here, the melting peak of GSF was also found in the thermograms of PULL/GSF NF and PULL/GSF-HPβCD-IC NF, demonstrating there was crystalline GSF in the samples. However, the peaks were reduced in intensity compared to pure GSF powder, and when comparing the two nanofibrous webs, it can be seen that the peak of the PULL/GSF-HPβCD-IC NF was broader than the peak of PULL/GSF NF. Figure S3

https://doi.org/10.1021/acs.molpharmaceut.3c00074
Mol. Pharmaceutics XXXX, XXX, XXX−XXX

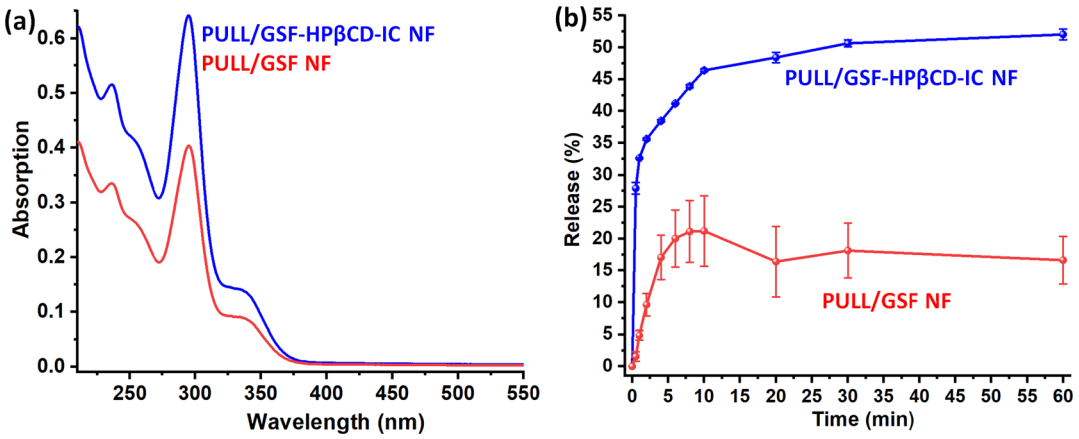

Figure 6. (a) UV−vis graphs and (b) *in vitro* time-dependent release profiles of PULL/GSF-HPβCD-IC NF and PULL/GSF NF.

indicated the expanded DSC thermogram of GSF, PULL/GSF-HPβCD-IC NF, and PULL/GSF NF. It was clear that, the melting peak of GSF in PULL/GSF-HPβCD-IC NF was broader compared to the GSF peak in the thermogram of PULL/GSF NF. Moreover, this endothermic peak was observed at a lower temperature (218.6 °C) than both PULL/GSF NF and pure GSF (219.4 °C). All these variations at the melting peak profile can be an indicator of the interaction between GSF and HPβCD in the case of PULL/GSF-HPβCD-IC NF since the inclusion complexation can lead to the broadening, reduction, absence, or shift at the melting point of drug molecules.[47]

The thermal profiles of samples were further studied using TGA (Figure S4). The TGA thermogram of GSF indicated a weight loss at 294 °C due to its thermal degradation. On the other hand, PULL/HPβCD and PULL/GSF-HPβCD-IC NF have two distinct weight losses, water evaporation up to 100 °C and PULL/HPβCD main degradation at ∼350 °C (Figure S4a). More clearly visible in the derivative thermograms is the difference in the degradation profile of the nanofibrous web by the incorporation of GSF into the PULL/HPβCD NF (Figure S4a-ii). Here, the degradation of PULL/HPβCD blend shifted to a lower temperature with a slight double peak (∼335 °C) and there was an additional weight loss step at 225 °C. The change in shape and temperature originated from the GSF content in the form of both crystalline and amorphous states that occurred by inclusion complexation. By contrast, the incorporation of GSF to the PULL NF did not change the main degradation profile and temperature of PULL (327 °C). For PULL/GSF NF, an additional step at 235 °C was detected due to crystalline GSF indicating the incorporation of the GSF in nanofibrous webs without an interaction (Figure S4b-ii). It is well-known that TGA findings can enable roughly calculating the weight ratio of each component within the sample. Depending on this, the weight loss steps corresponding to the GSF thermal degradation at the TGA thermograms of NFs and not overlapping with the thermal degradation of PULL or PULL/HPβCD was used to determine the approximate GSF content. Here, the GSF content was found to be ∼3.5 and ∼4.9% for PULL/GSF-HPβCD-IC NF and PULL/HPβCD, respectively. The lower GSF content was detected in the case of PULL/GSF-HPβCD-IC NF since a part of the GSF thermal degradation step was overlaid by the degradation step of PULL/HPβCD as it was also explained above and obvious from the derivative thermogram of PULL/GSF-HPβCD-IC NF (Figure S4a-ii). Here, the detected GSF content of ∼3.5% in the TGA thermogram of PULL/GSF-HPβCD-IC NF can be considered as the drug part which did not interact with HPβCD cavities in a way of inclusion complexation.

3.5. In Vitro Release and Disintegration Profile. Here, PULL/GSF-HPβCD-IC NF and PULL/GSF NF showed loading efficiencies of 97.8 ± 2.3% and 72.4 ± 8.9%, which correspond to the GSF content of ∼6.4% (w/w) and ∼ 4.7% (w/w), respectively. The higher loading efficiency with HPβCD revealed the complexation of GSF with HPβCD that allowed for higher amounts of the drug to be incorporated into the NF. This finding supported the FTIR result in which a higher intensity was detected for the characteristic peaks of GSF in PULL/GSF-HPβCD-IC NF when compared to PULL/GSF NF. The results of the loading efficiency test almost fit with the TGA finding, as well. The GSF content of PULL/GSF NF was found to be ∼4.9% (w/w) which is rather close to ∼4.7% (w/w). When the TGA and loading efficiency test results of PULL/GSF-HPβCD-IC NF were evaluated together, it was concluded that ∼48% of the GSF content of this nanofibrous web was amorphized due to inclusion complexation, and so ∼52% of GSF was in the crystal state. This is also correlated with the electrospinning solution photo (Figure 3c) and XRD graph (Figure 5a) which confirmed the existence of GSF crystals in PULL/GSF-HPβCD-IC NF. On the other hand, the heterogeneity originated from the uncomplexed/crystal drug content in the electrospinning solutions probably inhibiting the proper removal of these solutions from the vials to syringes and this resulted in a lack of including the whole initial GSF content during the electrospinning process. Briefly, this can be the explanation for the lower loading efficiency of PULL/GSF NF (∼4.7% (w/w)) compared to PULL/GSF-HPβCD-IC NF (∼6.4% (w/w)).

The dissolution behavior of GSF with/without HPβCD was checked using UV−vis spectroscopy, and the graphs are shown in Figure 6a. The absorption of GSF was detected higher when the IC was present in the nanofibrous webs. Here, the PULL/GSF-HPβCD-IC NF showed 1.28 ± 0.02 times higher absorption when compared to PULL/GSF NF. The higher absorption intensity also confirms the presence of inclusion complexation between GSF and HPβCD which provides higher solubility for GSF. Figure 6b displays the time-dependent release profiles of PULL/GSF-HPβCD-IC and PULL/GSF NF. PULL/GSF-HPβCD-IC NF had a higher and

https://doi.org/10.1021/acs.molpharmaceut.3c00074
Mol. Pharmaceutics XXXX, XXX, XXX−XXX

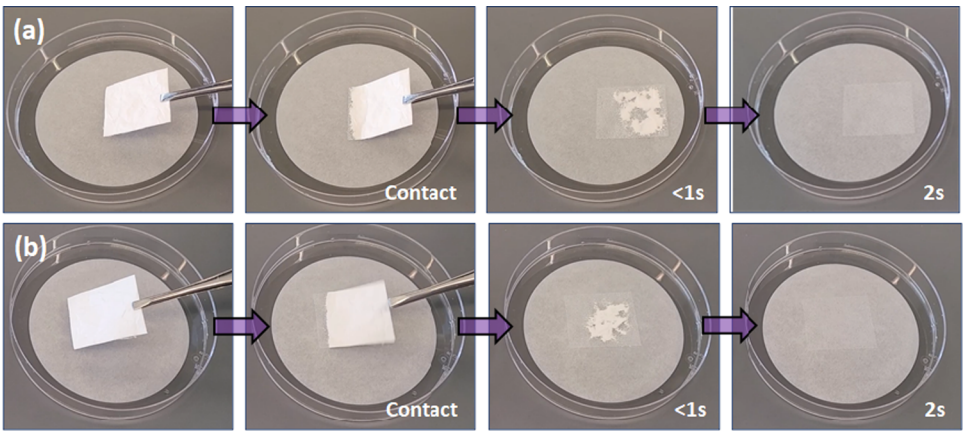

Figure 7. Disintegration behavior of (a) PULL/GSF-HPβCD-IC NF and (b) PULL/GSF NF.

faster release than PULL/GSF NF, reaching ~32% of release in just one minute, and its maximum release of ~52% in the first 20 min after which it had a steady release profile for the remainder of an hour. In comparison, the PULL/GSF NF reached a maximum of ~21% in the first 10 min, where it plateaued and did not release any more of the loaded drug. It was clear that the release of PULL/GSF-HPβCD-IC NF was much higher and consistent with the HPβCD, owing to the enhanced solubility of GSF due to inclusion complexation. The statistical analyses also suggested the significant differences between PULL/GSF-HPβCD-IC NF and PULL/GSF NF ($p < 0.05$).

Different kinetic models were also applied to further evaluate the release profile of electrospun nanofibrous webs. The formulas for calculation, the plotted graphs, and correlation coefficient values (R^2) are specified in Supporting Information (Table S1 and Figure S5). The results displayed that the release profile of both PULL/GSF-HPβCD-IC NF and PULL/GSF NF fit neither zero/first order nor Higuchi models (as provided in Table S1). This finding exhibited that GSF did not release with a time dependent way from an insoluble matrix (Fick's first law).[48] However, relatively higher R^2 values were found for the kinetic model of Korsmeyer−Peppas compared to others for both nanofibrous webs. This supported the erosion-based and diffusion-controlled release of GSF from nanofibrous webs. In addition, the slope of the fitted graphs of Korsmeyer−Peppas equations gives the diffusion exponent (n) value, and it was detected in the range of $n < 0.45$ pointing to the quasi-Fickian diffusion profile of samples (Table S1).[48,49]

The disintegration behavior of the nanofibrous webs was assessed in an artificial saliva simulation formed with wetted filter paper (Figure 7). Both PULL/GSF-HPβCD-IC NF and PULL/GSF NF were absorbed and disintegrated in 2 s (Figure 7). The fast-disintegration feature of nanofibrous webs revealed their suitability as a fast-disintegrating delivery system for oral administration. They would disintegrate rapidly in the oral cavity without a grainy feeling left behind upon treatment. While both PULL/GSF-HPβCD-IC NF and PULL/GSF NF disintegrated rapidly, the PULL/GSF-HPβCD-IC NF would be better suited for a FDDS given the fact that a higher amount of drug can be loaded into the system, released, and dissolved due to inclusion complexation with HPβCD.

4. CONCLUSIONS

Here, defect-free and self-standing nanofibrous webs of PULL/GSF-HPβCD-IC NF were successfully produced via electrospinning. The IC of GSF and HPβCD was formed with a 1:2 molar ratio (drug:CD) depending on the finding of the computational modeling study and this stoichiometry enabled to obtain PULL/GSF-HPβCD-IC NF efficiently. The control sample of PULL/GSF NF was produced for comparative studies. PULL/GSF-HPβCD-IC NF was produced having a much higher loading efficiency (~98%) compared to PULL/GSF NF (~72%), which further reveals the positive effect of inclusion complexation on drug encapsulation effectiveness. The amorphization of GSF provided an enhanced water-solubility for the drug molecules encapsulated into nanofibrous webs. Furthermore, more rapid and higher amount of GSF release from PULL/GSF-HPβCD-IC NF was accomplished compared to PULL/GSF NF. Both PULL/GSF-HPβCD-IC NF and PULL/GSF NF nanofibrous webs disintegrated rapidly in an artificial saliva environment (~2 s). Here, NFs being porous and having a very high surface area, the enhanced water-solubility of GSF by HPβCD inclusion complexation, and the choice of the highly water-soluble PULL matrix make PULL/GSF-HPβCD-IC NF a promising candidate for the development of innovative orally FDDSs. In addition, the improved aqueous solubility and release and fast-disintegration feature of PULL/GSF-HPβCD-IC NF can eliminate the unpleasant graininess feeling which can be easily observed in the case of orally disintegrating tablets. Additionally, the fragile and brittle feature of these tablets might not be a problem anymore due to the flexible and self-standing substrate structure of nanofibrous webs. The use of water only during the production of the nanofibrous web is also a noteworthy advantage of this approach in which any other toxic solvent or chemical was not required essentially. To conclude, PULL/GSF-HPβCD-IC NF formed by the combination of the IC and biopolymer (PULL) can be an attractive dosage formulation as an orally FDDS to ensure effective antifungal treatment.

■ ASSOCIATED CONTENT

Supporting Information

The Supporting Information is available free of charge at https://pubs.acs.org/doi/10.1021/acs.molpharmaceut.3c00074.

https://doi.org/10.1021/acs.molpharmaceut.3c00074
Mol. Pharmaceutics XXXX, XXX, XXX−XXX

Phase solubility, DSC and TGA graphs of samples, photos of NFs after long-term storage, and release kinetics calculations and result (PDF)

Comparative disintegration profile of PULL/GSF-HPβCD-IC NF and PULL/GSF NF (MP4)

AUTHOR INFORMATION

Corresponding Authors

Asli Celebioglu − *Fiber Science Program, Department of Human Centered Design, College of Human Ecology, Cornell University, Ithaca, New York 14853, United States;* orcid.org/0000-0002-5563-5746; Email: ac2873@cornell.edu

Tamer Uyar − *Fiber Science Program, Department of Human Centered Design, College of Human Ecology, Cornell University, Ithaca, New York 14853, United States;* orcid.org/0000-0002-3989-4481; Email: tu46@cornell.edu

Authors

Emmy Hsiung − *Fiber Science Program, Department of Human Centered Design, College of Human Ecology, Cornell University, Ithaca, New York 14853, United States*

Mehmet Emin Kilic − *Computational Science Research Center, Korea Institute of Science and Technology, Seoul 02792, Republic of Korea*

Engin Durgun − *UNAM-National Nanotechnology Research Center and Institute of Materials Science and Nanotechnology, Bilkent University, Ankara 06800, Turkey;* orcid.org/0000-0002-0639-5862

Complete contact information is available at: https://pubs.acs.org/10.1021/acs.molpharmaceut.3c00074

Author Contributions

E.H.: Investigation, Writing-original draft; A.C.: Conceptualization, Methodology, Investigation, Writing-original draft, Review & editing; M.E.K.: Performing computational modeling; E.D.: Formal analysis and methodology of computational modeling part, Writing & editing of computational modeling part; T.U.: Conceptualization, Formal analysis, Methodology, Writing - review & editing, Supervision, Project administration. E.H. and A.C. contributed equally.

Notes

The authors declare no competing financial interest.

ACKNOWLEDGMENTS

This work made use of: Department of Human Centered Design facilities, Cornell Center for Materials Research (CCMR) supported by NSF MRSEC (DMR-1719875), Cornell Chemistry NMR Facility supported in part by the NSF MRI program (CHE-1531632). M.E.K. acknowledges National Research Foundation of Korea (NRF) of Brain Pool Program funded by the Ministry of Science and ICT (2020H1D3A1A02081517).

REFERENCES

(1) Jain, K. K. An Overview of Drug Delivery Systems. *Drug Delivery Syst.* **2020**, *2059*, 1−54.

(2) Preis, M. Orally Disintegrating Films and Mini-Tablets—Innovative Dosage Forms of Choice for Pediatric Use. *AAPS PharmSciTech* **2015**, *16*, 234−241.

(3) He, M.; Zhu, L.; Yang, N.; Li, H.; Yang, Q. Recent Advances of Oral Film as Platform for Drug Delivery. *Int. J. Pharm.* **2021**, *604*, No. 120759.

(4) Laffleur, F.; Keckeis, V. Advances in Drug Delivery Systems: Work in Progress Still Needed? *Int. J. Pharm.* **2020**, *590*, No. 119912.

(5) Luraghi, A.; Peri, F.; Moroni, L. Electrospinning for Drug Delivery Applications: A Review. *J. Controlled Release* **2021**, *334*, 463−484.

(6) Balusamy, B.; Celebioglu, A.; Senthamizhan, A.; Uyar, T. Progress in the Design and Development of "Fast-Dissolving" Electrospun Nanofibers Based Drug Delivery Systems - A Systematic Review. *J. Controlled Release* **2020**, *326*, 482−509.

(7) Bai, Y.; Wang, D.; Zhang, Z.; Pan, J.; Cui, Z.; Yu, D.-G.; Bligh, S.-W. A. Testing of Fast Dissolution of Ibuprofen from Its Electrospun Hydrophilic Polymer Nanocomposites. *Polym. Test.* **2021**, *93*, No. 106872.

(8) Celebioglu, A.; Tekant, D.; Kilic, M. E.; Durgun, E.; Uyar, T. Orally Fast-Disintegrating Resveratrol/Cyclodextrin Nanofibrous Films as a Potential Antioxidant Dietary Supplement. *ACS Food Sci. Technol.* **2022**, *2*, 568−580.

(9) Illangakoon, U. E.; Gill, H.; Shearman, G. C.; Parhizkar, M.; Mahalingam, S.; Chatterton, N. P.; Williams, G. R. Fast Dissolving Paracetamol/Caffeine Nanofibers Prepared by Electrospinning. *Int. J. Pharm.* **2014**, *477*, 369−379.

(10) Wang, Y.; Deng, Z.; Wang, X.; Shi, Y.; Lu, Y.; Fang, S.; Liang, X. Formononetin/Methyl-β-Cyclodextrin Inclusion Complex Incorporated into Electrospun Polyvinyl-Alcohol Nanofibers: Enhanced Water Solubility and Oral Fast-Dissolving Property. *Int. J. Pharm.* **2021**, *603*, No. 120696.

(11) Sood, A.; Gupta, A.; Agrawal, G. Recent Advances in Polysaccharides Based Biomaterials for Drug Delivery and Tissue Engineering Applications. *Carbohydr. Polym. Technol. Appl.* **2021**, *2*, No. 100067.

(12) Seif, S.; Franzen, L.; Windbergs, M. Overcoming Drug Crystallization in Electrospun Fibers−Elucidating Key Parameters and Developing Strategies for Drug Delivery. *Int. J. Pharm.* **2015**, *478*, 390−397.

(13) Singh, R. S.; Kaur, N.; Singh, D.; Bajaj, B. K.; Kennedy, J. F. Downstream Processing and Structural Confirmation of Pullulan—A Comprehensive Review. *Int. J. Biol. Macromol.* **2022**, *208*, 553−564.

(14) Singh, R. S.; Kaur, N.; Singh, D.; Purewal, S. S.; Kennedy, J. F. Pullulan in Pharmaceutical and Cosmeceutical Formulations: A Review. *Int. J. Biol. Macromol.* **2023**, *231*, No. 123353.

(15) Asgari, S.; Pourjavadi, A.; Setayeshmehr, M.; Boisen, A.; Ajalloueian, F. Encapsulation of Drug-Loaded Graphene Oxide-Based Nanocarrier into Electrospun Pullulan Nanofibers for Potential Local Chemotherapy of Breast Cancer. *Macromol. Chem. Phys.* **2021**, *222*, No. 2100096.

(16) Pang, H.; Tian, K.; Li, Y.; Su, C.; Duan, F.; Xu, Y. Super-Hydrophobic PTFE Hollow Fiber Membrane Fabricated by Electrospinning of Pullulan/PTFE Emulsion for Membrane Deamination. *Sep. Purif. Technol.* **2021**, *274*, No. 118186.

(17) Atila, D.; Keskin, D.; Tezcaner, A. Crosslinked Pullulan/Cellulose Acetate Fibrous Scaffolds for Bone Tissue Engineering. *Mater. Sci. Eng. C* **2016**, *69*, 1103−1115.

(18) Celebioglu, A.; Uyar, T. Electrohydrodynamic Encapsulation of Eugenol-Cyclodextrin Complexes in Pullulan Nanofibers. *Food Hydrocolloids* **2021**, *111*, No. 106264.

(19) Duan, M.; Yu, S.; Sun, J.; Jiang, H.; Zhao, J.; Tong, C.; Hu, Y.; Pang, J.; Wu, C. Development and Characterization of Electrospun Nanofibers Based on Pullulan/Chitin Nanofibers Containing Curcumin and Anthocyanins for Active-Intelligent Food Packaging. *Int. J. Biol. Macromol.* **2021**, *187*, 332−340.

(20) Soto, K. M.; Hernández-Iturriaga, M.; Loarca-Piña, G.; Luna-Bárcenas, G.; Mendoza, S. Antimicrobial Effect of Nisin Electrospun Amaranth: Pullulan Nanofibers in Apple Juice and Fresh Cheese. *Int. J. Food Microbiol.* **2019**, *295*, 25−32.

(21) Chang, H.; Xu, J.; Macqueen, L. A.; Aytac, Z.; Peters, M. M.; Zimmerman, J. F.; Xu, T.; Demokritou, P.; Parker, K. K. High-

Throughput Coating with Biodegradable Antimicrobial Pullulan Fibres Extends Shelf Life and Reduces Weight Loss in an Avocado Model. *Nat. Food* **2022**, *3*, 428−436.
(22) Qin, Z.; Jia, X.-W.; Liu, Q.; Kong, B.; Wang, H. Fast Dissolving Oral Films for Drug Delivery Prepared from Chitosan/Pullulan Electrospinning Nanofibers. *Int. J. Biol. Macromol.* **2019**, *137*, 224−231.
(23) Hsiung, E.; Celebioglu, A.; Chowdhury, R.; Kilic, M. E.; Durgun, E.; Altier, C.; Uyar, T. Antibacterial Nanofibers of Pullulan/Tetracycline-Cyclodextrin Inclusion Complexes for Fast-Disintegrating Oral Drug Delivery. *J. Colloid Interface Sci.* **2022**, *610*, 321−333.
(24) Braga, S. S. Cyclodextrin Superstructures for Drug Delivery. *J. Drug Delivery Sci. Technol.* **2022**, *75*, No. 103650.
(25) Crini, G. A History of Cyclodextrins. *Chem. Rev.* **2014**, *114*, 10940−10975.
(26) Carneiro, S. B.; Duarte, C.; Ílary, F.; Heimfarth, L.; Quintans, S.; de Souza, J.; Quintans-Júnior, L. J.; da Veiga Júnior, V. F.; Neves de Lima, Á. A. Cyclodextrin−Drug Inclusion Complexes: In Vivo and In Vitro Approaches. *Int. J. Mol. Sci.* **2019**, *20*, 642.
(27) Jansook, P.; Ogawa, N.; Loftsson, T. Cyclodextrins: Structure, Physicochemical Properties and Pharmaceutical Applications. *Int. J. Pharm.* **2018**, *535*, 272−284.
(28) Li, Z.; Li, K.; Teng, M.; Li, M.; Sui, X.; Liu, B.; Tian, B.; Fu, Q. Functionality-Related Characteristics of Hydroxypropyl-β-Cyclodextrin for the Complexation. *J. Mol. Liq.* **2022**, *365*, No. 120105.
(29) Gould, S.; Scott, R. C. 2-Hydroxypropyl-β-Cyclodextrin (HP-β-CD): A Toxicology Review. *Food Chem. Toxicol.* **2005**, *43*, 1451−1459.
(30) Li, P.; Song, J.; Ni, X.; Guo, Q.; Wen, H.; Zhou, Q.; Shen, Y.; Huang, Y.; Qiu, P.; Lin, S.; Hu, H. Comparison in Toxicity and Solubilizing Capacity of Hydroxypropyl-β-Cyclodextrin with Different Degree of Substitution. *Int. J. Pharm.* **2016**, *513*, 347−356.
(31) Celebioglu, A.; Uyar, T. Metronidazole/Hydroxypropyl-β-Cyclodextrin Inclusion Complex Nanofibrous Webs as Fast-Dissolving Oral Drug Delivery System. *Int. J. Pharm.* **2019**, *572*, No. 118828.
(32) Celebioglu, A.; Uyar, T. Electrospun Formulation of Acyclovir/Cyclodextrin Nanofibers for Fast-Dissolving Antiviral Drug Delivery. *Mater. Sci. Eng. C* **2021**, *118*, No. 111514.
(33) Hsiung, E.; Celebioglu, A.; Kilic, M. E.; Durgun, E.; Uyar, T. Ondansetron/Cyclodextrin Inclusion Complex Nanofibrous Webs for Potential Orally Fast-Disintegrating Antiemetic Drug Delivery. *Int. J. Pharm.* **2022**, *623*, No. 121921.
(34) Celebioglu, A.; Wang, N.; Kilic, M. E.; Durgun, E.; Uyar, T. Orally Fast Disintegrating Cyclodextrin/Prednisolone Inclusion-Complex Nanofibrous Webs for Potential Steroid Medications. *Mol. Pharmaceutics* **2021**, *18*, 4486−4500.
(35) Kumar, R. Nanotechnology Based Approaches to Enhance Aqueous Solubility and Bioavailability of Griseofulvin: A Literature Survey. *J. Drug Delivery Sci. Technol.* **2019**, *53*, No. 101221.
(36) Omar, S. M.; Ibrahim, F.; Ismail, A. Formulation and Evaluation of Cyclodextrin-Based Nanosponges of Griseofulvin as Pediatric Oral Liquid Dosage Form for Enhancing Bioavailability and Masking Bitter Taste. *Saudi Pharm. J.* **2020**, *28*, 349−361.
(37) Lopez, F. L.; Shearman, G. C.; Gaisford, S.; Williams, G. R. Amorphous Formulations of Indomethacin and Griseofulvin Prepared by Electrospinning. *Mol. Pharmaceutics* **2014**, *11*, 4327−4338.
(38) Olson, J. M.; Troxell, T. Griseofulvin. In *StatPearls [Internet]*; StatPearls Publishing, 2022.
(39) Veiga, M. D.; Díaz, P. J.; Ahsan, F. Interactions of Griseofulvin with Cyclodextrins in Solid Binary Systems. *J. Pharm. Sci.* **1998**, *87*, 891−900.
(40) Kresse, G.; Furthmüller, J. Efficiency of Ab-Initio Total Energy Calculations for Metals and Semiconductors Using a Plane-Wave Basis Set. *Comput. Mater. Sci.* **1996**, *6*, 15−50.
(41) Grimme, S. Semiempirical GGA-type Density Functional Constructed with a Long-range Dispersion Correction. *J. Comput. Chem.* **2006**, *27*, 1787−1799.
(42) Mathew, K.; Sundararaman, R.; Letchworth-Weaver, K.; Arias, T. A.; Hennig, R. G. Implicit Solvation Model for Density-Functional Study of Nanocrystal Surfaces and Reaction Pathways. *J. Chem. Phys.* **2014**, *140*, 84106.
(43) Higuchi, T.; Connors, K. A. Phase Solubility Diagram. *Adv. Anal. Chem. Instrum.* **1965**, *4*, 117−212.
(44) Xue, J.; Wu, T.; Dai, Y.; Xia, Y. Electrospinning and Electrospun Nanofibers: Methods, Materials, and Applications. *Chem. Rev.* **2019**, *119*, 5298−5415.
(45) Yuan, C.; Liu, B.; Liu, H. Characterization of Hydroxypropyl-β-Cyclodextrins with Different Substitution Patterns via FTIR, GC−MS, and TG−DTA. *Carbohydr. Polym.* **2015**, *118*, 36−40.
(46) Yang, Y.; Xie, B.; Liu, Q.; Kong, B.; Wang, H. Fabrication and Characterization of a Novel Polysaccharide Based Composite Nanofiber Films with Tunable Physical Properties. *Carbohydr. Polym.* **2020**, *236*, No. 116054.
(47) Narayanan, G.; Boy, R.; Gupta, B. S.; Tonelli, A. E. Analytical Techniques for Characterizing Cyclodextrins and Their Inclusion Complexes with Large and Small Molecular Weight Guest Molecules. *Polym. Test.* **2017**, *62*, 402−439.
(48) Peppas, N. A.; Narasimhan, B. Mathematical Models in Drug Delivery: How Modeling Has Shaped the Way We Design New Drug Delivery Systems. *J. Controlled Release* **2014**, *190*, 75−81.
(49) Li, X.; Kanjwal, M. A.; Lin, L.; Chronakis, I. S. Electrospun Polyvinyl-Alcohol Nanofibers as Oral Fast-Dissolving Delivery System of Caffeine and Riboflavin. *Colloids Surf., B* **2013**, *103*, 182−188.

https://doi.org/10.1021/acs.molpharmaceut.3c00074
Mol. Pharmaceutics XXXX, XXX, XXX−XXX